A Novel Precision Measuring Parallel Mechanism for the Closed-Loop Control of a Biologically Inspired Lower Limb Exoskeleton

Zhou, Libo; Chen, Weihai; Wang, Jianhua; Bai, Shaoping; Yu, Haoyong; Zhang, Yinping

Published in:
IEEE/ASME Transactions on Mechatronics

DOI (link to publication from Publisher):
10.1109/TMECH.2018.2872011

Publication date:
2018

Document Version
Accepted author manuscript, peer reviewed version

This article has been accepted for publication in a future issue of this journal, but has not been fully edited. Content may change prior to final publication. Citation information: DOI 10.1109/TMECH.2018.2872011, IEEE/ASME Transactions on Mechatronics

A Novel Precision Measuring Parallel Mechanism for the Closed-loop Control of a Biologically Inspired Lower Limb Exoskeleton

Libo Zhou, Weihai Chen*, *Member, IEEE*, Jianhua Wang, Shaoping Bai, *Member, IEEE*, Haoyong Yu, *Member, IEEE,* and Yinping Zhang

***Abstract*—The knee joint of the human body involves both rotation and translation, while the magnitude of anterior-posterior translation during flexion/extension movement of the knee joint is very small compared with the length of the human lower limb. It is therefore desirable for an exoskeleton leg to have two degrees of freedom to accommodate the motion of the human knee joint, and for there to be a precision measuring method to obtain its trajectory. This paper presents a novel parallel mechanism which can be used as a precise measuring device to realize closed-loop control for a biologically inspired 3-degree of freedom (DOF) lower limb exoskeleton (BLLE-3) for human gait rehabilitation. In this work, mechanical design and kinematics of the exoskeleton are described. Errors of exoskeleton motion are modelled and analyzed. Closed-loop control law is implemented to enable accurate trajectory following the motions of the exoskeleton. Simulations and experimental results are included to show the effectiveness of the new measuring and control method.**

***Index Terms*—Precision measuring, parallel mechanism, closed-loop control, lower limb exoskeleton, errors.**

I. Introduction

MILLIONS of people worldwide suffer from neurological disorders such as stroke, Parkinson's disease, and cerebral palsy which lead to movement problems. These problems not only render the patients incapable of performing normal daily activities, but also have a big impact on their families and social welfare services. As the population ages, more and more patients suffer motor disturbances because of age-related diseases [1]. Medical research shows that repetitive and task-oriented functional training can help patients rebuild the relevant functions of the nervous system [2]. Traditional treatments performed by physical therapists and medical personnel are time and labor intensive. By comparison, rehabilitation robots are able to perform gait therapy effectively and economically for physically impaired patients. Furthermore, rehabilitation robots can monitor and assess patients' status with built-in sensors and increase the accuracy of treatment tasks repeated many times. Thus, the need for rehabilitation robots is steadily increasing [3]-[6].

Rehabilitation robots have been developed for either the upper limbs or the lower limbs, and the latter are used mainly for helping patients with lower limb movement dysfunctions. Based on the driving principles, the robots can be grouped into endpoint manipulators and powered exoskeletons [7]. The endpoint manipulators for lower limbs have footplates that are mounted on the robots, such as MGT [8], GM2 [9], HapticWalker [10] and G-EO Systems [11]. They need only provide foot trajectory in training which indirectly generates joint motions of the lower limbs and not to be accurately aligned with the joints. They also allow dexterous ankle movements for users that are able to move their hip and knee joints by themselves. Therefore, they are effective in encouraging a user's motivation, but the task of maintaining the user's balance is challenging [12] [13]. Lower limb exoskeletons, such as Lokomat [14], LOPES [15], WalkTrainer [16], ALEX III [17], ReWalk [18] and HAL [19], run parallel to the human lower limbs, with the actuator and sensors installed directly on the joints. These exoskeletons can be controlled separately at joints to meet different rehabilitation training requirements. However, the joint alignment between human and exoskeleton is challenging, for reasons of both exoskeleton design and human joint anatomy. If misalignment occurs, patients will feel uncomfortable [20].

One of the reasons for misalignment between the exoskeleton and the human is that human joints are complex. For example, the human knee joint, which is considered as a revolute joint in most rehabilitation exoskeleton designs, is a joint involving both rotation and translation. At the knee joint, the center of rotation changes in the process of rotating in the sagittal plane, as shown in Fig. 1 [21], [22]. Some designs have addressed this problem by adding extra passive degrees of freedom (DOFs) [23]-[25] to adapt to the joint misalignments. However, the joint alignments are uncontrolled, which leads to additional uncompensated mechanical impedance [26] and the efficiency of the force transfer will be reduced. In [27], a knee exoskeleton with 3 active DOFs in the sagittal is proposed. It can allow for translations while assisting flexion-extension movement of the knee. The main drawback is the mechanism looks heavy and complex. A bio-joint cam mechanism was proposed in [28]. While the mechanism can closely match the motion of human knee joint, an off-line adjustment is needed for every individual, which is a tedious process.

Considering that the coupling motions in human knee joints, namely, rolling along with sliding motions which are performed by multiple skeletal muscles pulling bones and moving the bones around the surface of the knee joint, a parallel structure (similar to multiple skeletal muscles) will have a special significance in the bionic design of knee joints. To this end, a planar 3-DOF parallel mechanism model has been proposed, in which the hip joint has one DOF and the virtual knee joint has two DOFs in the sagittal plane. The bionic knee joint mechanism is realized by a simple structure with two linear actuators [29]. This mechanism shows some advantages in generating motion matching the human knee joints, but the realization of an accurate trajectory control is challenging for the relative short range of sliding motion.

This research was supported by the National Natural Science Foundation of China under Grant 61773042, 61573047 and 51675018.

Libo Zhou, Weihai Chen*, Jianhua Wang and Yinping Zhang are with the School of Automation Science and Electrical Engineering, Beihang University, BJ 100191, China (E-mail: libozhou@buaa.edu.cn; whchen@buaa.edu.cn; jhwangbuaa@126.com; ping0209@163.com)

Shaoping Bai is with the Department of Materials and Production, Aalborg University, Aalborg 9220, Denmark (shb@mp.aau.dk)

Haoyong Yu is with the Department of Biomedical Engineering, National University of Singapore, SG 117575, Singapore (bieyhy@nus.edu.sg).

This article has been accepted for publication in a future issue of this journal, but has not been fully edited. Content may change prior to final publication. Citation information: DOI 10.1109/TMECH.2018.2872011, IEEE/ASME Transactions on Mechatronics

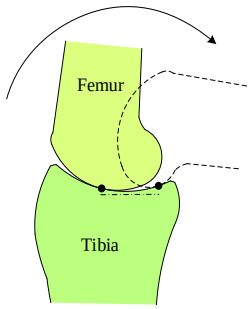

Fig. 1. Schematic representation of the knee joint rolling and sliding in the sagittal plane.

It has been noted that the magnitude of anterior posterior translation of the knee joint is about 19 mm for a healthy human [30]. This is very small compared to the length of a human shank. The amount of translation changes with the flexion and extension angle and the relation between them is unique to every individual, since it strongly depends on the size and orientation of the bones and the shape of articulated surfaces. Therefore, it is desirable to design a 2-DOF knee mechanism together with a precise measuring mechanism to obtain the lower limb trajectory. Otherwise, it will be difficult for the exoskeleton to perform a trajectory that can well fit the complex coupled motion of the human knee joint. In this work, we present a novel and compact lower limb exoskeleton robot, which is built with a 3-RPR (Revolute – Prismatic – Revolute pairs) parallel mechanism to generate the coupling motions at the human knee joint and also to measure the trajectories of the human lower limb precisely in order to realize a closed loop control of the exoskeleton.

In this paper, the kinematic design and modeling of the exoskeleton is presented with focus on the 3-RPR mechanism. Error models of the exoskeleton are developed. A closed-loop control law of the exoskeleton is developed for precise trajectory control. Simulations are conducted to show the performance of the new design. Experiments on the prototype demonstrate the feasibility of the exoskeleton.

II. Kinematic Design and Modeling

A kinematic representation of the lower limb exoskeleton robot is shown in Fig. 2. It has a 1-DOF hip joint module and a 2-DOF knee joint module. The hip joint is driven by a linear actuator to complete a pure rotation. As for the knee joint, a parallel mechanism, namely, the 3-RPR mechanism to generate 2-DOF motion, has been designed, as shown in Fig. 3. Of the three RPR sub-chains, two are active and used to drive the knee joint movement, while one RPR branch chain is passive and used for measuring the motion trajectory.

The exoskeleton design considers the mechanism adjustability to fit people of different sizes. A lead screw nut mechanism allowing the adjustment of the thigh length is shown in Fig. 4 (a). For the adjustment of the shank length, a two-stage adjusting mechanism was designed. As shown in Fig. 4 (b), the adjusting slider can be fixed in different places in the adjusting mechanism to realize a wide range of gross adjustments. Moreover, a guide rail with slider can adapt precisely to different lengths in a short range as seen in Fig. 4 (c).

Referring to the kinematic model shown in Fig. 2 (b), l_0, l_1, l_2 are lengths of three actuators, and θ_1 and $\theta_{\text{knee}} = \theta_2 - \theta_3$ are angles of rotation at the hip and knee joints. The fixed- coordinate frame $x - O_2 - y$ is defined with its origin located at point O_2.

From Fig. 2 (b), we get the solutions of θ_1 and its time derivative.

$$\begin{cases} \theta_1 = \dfrac{\pi}{2} - \delta_1 - \delta_2 - \cos^{-1}\left(\dfrac{{d_1}^2 + {d_2}^2 - {l_0}^2}{2d_1 d_2}\right) \\ \dot{\theta}_1 = \dfrac{-4d_1 d_2 l_0}{\sqrt{[(d_1+d_2)^2 - {l_0}^2][{l_0}^2 - (d_1-d_2)^2]}}\dot{l}_0 . \end{cases} \quad (1)$$

For the inverse kinematics of the hip joint, we get

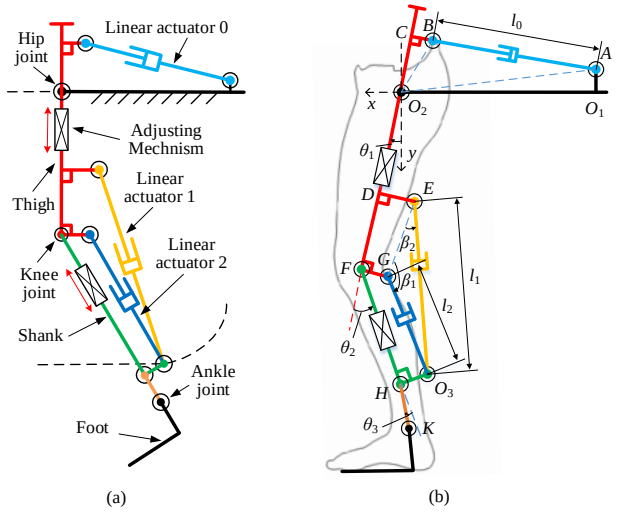

Fig. 2. Model of lower limb exoskeleton robot: (a) structural diagram, (b) kinematic model.

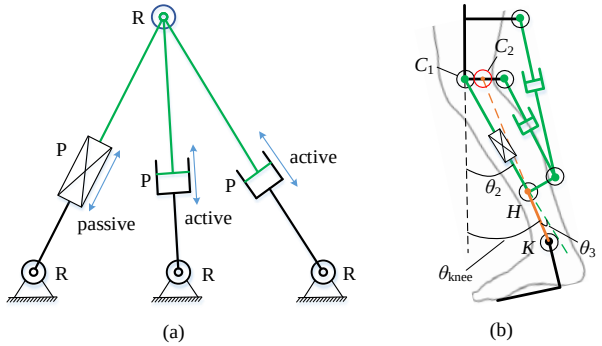

Fig. 3. 2 DOF 3-RPR parallel mechanism: (a) structural diagram, (b) working principle. C_1 and C_2 are instantaneous centers of rotation of link *HK* with respect to knee joint rotation angles equal to zero and an arbitrary value.

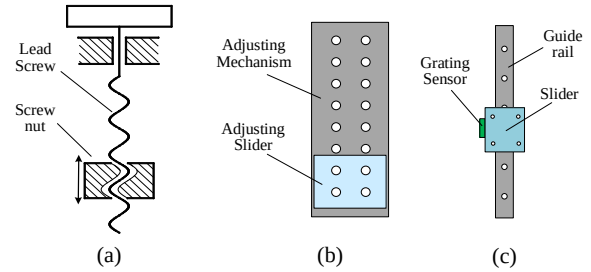

Fig. 4. Adjusting mechanisms: (a) thigh length adjustment, (b) gross shank length adjustment, (c) fine shank length adjustment.

This article has been accepted for publication in a future issue of this journal, but has not been fully edited. Content may change prior to final publication. Citation information: DOI 10.1109/TMECH.2018.2872011, IEEE/ASME Transactions on Mechatronics

$$\begin{cases} l_0 = \sqrt{{d_1}^2 + {d_2}^2 - 2d_1 d_2 \sin(\delta_1 + \delta_2 + \theta_1)} \\ \dot{l}_0 = \dfrac{-d_1 d_2 \cos(\delta_1 + \delta_2 + \theta_1)}{\sqrt{{d_1}^2 + {d_2}^2 - 2d_1 d_2 \sin(\delta_1 + \delta_2 + \theta_1)}}\,\dot{\theta}_1, \end{cases} \tag{2}$$

where $\delta_1 = \angle CO_2B$, $\delta_2 = \angle AO_2O_1$, $d_1 = l_{O_2A}$, $d_2 = l_{O_2B}$, which are all fixed.

The position of point O_3, namely, the knee joint driving point can be found as [29]

$$\begin{cases} x_{O_3} = \dfrac{[x_E - k(p - y_E)] - m}{k^2 + 1} \\ y_{O_3} = k\dfrac{[x_E - k(p - y_E)] - m}{k^2 + 1} + p\,, \end{cases} \tag{3}$$

where (x_{O_3}, y_{O_3}) is the coordinate of O_3, (x_E, y_E) and (x_G, y_G) are the coordinates of points E and G, respectively, and

$$k = -(x_G - x_E)/(y_G - y_E),$$

$$p = [{l_1}^2 - {l_2}^2 + ({x_G}^2 - {x_E}^2) + ({y_G}^2 - {y_E}^2)]/[2(y_G - y_E)],$$

$$m = \sqrt{[k(p - y_E) - x_E]^2 - (k^2 + 1)[{x_E}^2 + (p - y_E)^2 - l_1]}.$$

For the inverse kinematics of the knee joint, we can obtain

$$\begin{cases} l_1 = \sqrt{(x_{O_3} - x_E)^2 + (y_{O_3} - y_E)^2} \\ l_2 = \sqrt{(x_{O_3} - x_G)^2 + (y_{O_3} - y_G)^2}\,. \end{cases} \tag{4}$$

Let $q = [l_1\ l_2]^T$ and $x = [x_{O_3}\ y_{O_3}]^T$, (4) yields [29]

$$J_x \dot{x} = J_q \dot{q}, \tag{5}$$

where $J_x = \begin{bmatrix} (x_{O_3} - x_E) & (y_{O_3} - y_E) \\ (x_{O_3} - x_G) & (y_{O_3} - y_G) \end{bmatrix}$ and $J_q = \begin{bmatrix} l_1 & 0 \\ 0 & l_2 \end{bmatrix}$. The overall Jacobian matrix, J, can be written as $\dot{q} = J\dot{x}$, where $J = {J_q}^{-1} J_x$.

Since matrix J_q is not singular, the overall Jacobian matrix for the knee joint is:

$$J = {J_q}^{-1} J_x = \begin{bmatrix} \dfrac{(x_{O_3} - x_E)}{l_1} & \dfrac{(y_{O_3} - y_E)}{l_1} \\ \dfrac{(x_{O_3} - x_G)}{l_2} & \dfrac{(y_{O_3} - y_G)}{l_2} \end{bmatrix}. \tag{6}$$

Moreover, the position of point O_3 can be calculated by (7) with θ_1, θ_2 and l_{FH} measured via sensors.

$$\begin{bmatrix} x'_{O_3} \\ y'_{O_3} \end{bmatrix} = \begin{bmatrix} -\sin\theta' & -\cos\theta' \\ \cos\theta' & -\sin\theta' \end{bmatrix} \begin{bmatrix} l_{FH} \\ l_{HO_3} \end{bmatrix} + \begin{bmatrix} x_F \\ y_F \end{bmatrix}, \tag{7}$$

where x'_{O_3} and y'_{O_3} are the measured coordinates of point O_3, $\theta' = \theta_2 - \theta_1$, l_{FH} is the adjustable length of FH and l_{HO_3} is the fixed length of HO_3.

The thigh is attached at O_2F and the calf is attached at HK. As shown in Figs. 2 (b) and 3 (b), the rotation angle of the knee joint θ_{knee} is equal to $\theta_2 - \theta_3$. As the magnitude of anterior-posterior translation during flexion/extension movement of the knee joint is very small (about 19mm) compared with the length of the human lower limb, we can infer that the value of θ_3 will also be very small. As θ_3 is close to zero, θ_2 is nearly identical to θ_{knee}.

III. Error Modeling and Analysis

A rehabilitation exoskeleton commonly needs to move in accordance with a predefined trajectory. In a closed-loop control, we need to obtain in real time the actual trajectory during movement. For this purpose, an absolute angle encoder is installed at the hip joint to obtain the actual value of θ_1. At the knee joint, because the magnitude of anterior posterior translation is very small compared with the length of the shank, a precise measurement is necessary. In this section, errors in the knee joint part will be analyzed.

Due to clearance and installation errors in the revolute joints, there are errors between the theoretical and actual dimensions and parameters [31]. As seen in Fig. 5, the dashed lines stand for the theoretical mechanical parameterizations and the solid lines for the actual mechanical ones. $(\Delta sx, \Delta sy)$, $(\Delta zx, \Delta zy)$ are geometric errors in points E and F, respectively. These errors are mainly due to assembly and manufacturing errors. Their effect on accuracy is usually measurable and repeatable, and thus can be eliminated by adjusting the parameters. $\Delta\beta_1$, $\Delta\beta_2$, $\Delta\theta_2$ are angle errors that are mainly due to clearances in the prismatic and revolute joints. Their influence on accuracy is not repeatable and they are difficult to model and eliminate. However, we tried to reduce their effect on accuracy.

A. The Original Measurement Method

A measuring method was proposed in [29], as demonstrated in Fig. 6. We first briefly presented the error model of this method to pinpoint the limitation of this method, prior to introducing our new solution.

Two absolute angle encoders are installed at joints located at E and G, from which angles β_1 and β_2 can be obtained, which yield further the values of l_1 and l_2 as

$$\begin{aligned} l_1 &= l_{GE} \cdot \frac{\sin\beta_1}{\sin\delta} \\ l_2 &= l_{GE} \cdot \frac{\sin\beta_2}{\sin\delta}, \end{aligned} \tag{8}$$

where $\delta = \pi - \beta_1 - \beta_2$, and l_{GE} is the length of GE.

The location of O_3 is found by

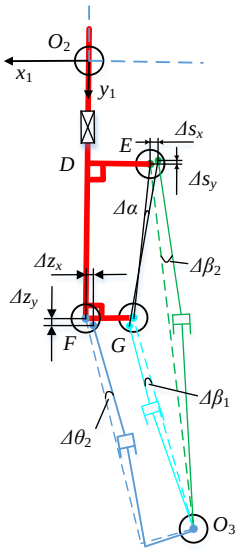

Fig. 5. Error model of the exoskeleton in the knee joint part.

This article has been accepted for publication in a future issue of this journal, but has not been fully edited. Content may change prior to final publication. Citation information: DOI 10.1109/TMECH.2018.2872011, IEEE/ASME Transactions on Mechatronics

$$\begin{bmatrix} x_{O_3} \\ y_{O_3} \end{bmatrix} = l_i \boldsymbol{u}_i + \begin{bmatrix} x_i \\ y_i \end{bmatrix}, \quad i = 1, 2, \tag{9}$$

with

$$\boldsymbol{u}_i = \begin{bmatrix} \cos\gamma_i \\ \sin\gamma_i \end{bmatrix}, \begin{bmatrix} \gamma_1 \\ \gamma_2 \end{bmatrix} = \begin{bmatrix} \alpha_1 + \beta_2 \\ \pi + \alpha_2 - \beta_1 \end{bmatrix}, \begin{bmatrix} x_1 \\ y_1 \end{bmatrix} = \begin{bmatrix} x_E \\ y_E \end{bmatrix}, \begin{bmatrix} x_2 \\ y_2 \end{bmatrix} = \begin{bmatrix} x_G \\ y_G \end{bmatrix},$$

where $[x_E,\ y_E]$, $[x_G,\ y_G]$ are the position coordinates of points E and G, respectively.

Equations (8) and (9) yield

$$\begin{bmatrix} x_{O_3} \\ y_{O_3} \end{bmatrix} = \frac{l_{GE}.\sin\beta_i}{\sin\delta} \cdot \begin{bmatrix} \cos\gamma_i \\ \sin\gamma_i \end{bmatrix} + \begin{bmatrix} x_i \\ y_i \end{bmatrix}, \quad i = 1, 2. \tag{10}$$

Any of the two sub-chains (i=1, 2) can yield the position coordinates of point O_3, and makes no difference in error analysis. Here, we select the first chain (i=1).

Upon differentiation of (10), the positioning error of point O_3 is obtained as

$$\Delta\boldsymbol{d} = \boldsymbol{J_l}\,\Delta l_{GE} + \boldsymbol{J_{\beta_1}}\Delta\beta_1 + \boldsymbol{J_{\beta_2}}\Delta\beta_2 + \boldsymbol{J_{\alpha_1}}\Delta\alpha_1 + \boldsymbol{J_s}\Delta s, \tag{11}$$

where, $\Delta\boldsymbol{d} = [\Delta x_{O_3}\ \Delta y_{O_3}]^T$ is the positioning error of point O_3, Δs is the position error of point E. As $\Delta l_{GE}, \Delta\alpha_1, \Delta s$ are geometric errors and they can be eliminated by adjusting the parameters. To simplify the analysis, only $\Delta\beta_1$ and $\Delta\beta_2$ are taken into consideration for further analysis. (11) can be reformulated as

$$\Delta\boldsymbol{d} = \boldsymbol{J_{\beta_1}}\Delta\beta_1 + \boldsymbol{J_{\beta_2}}\Delta\beta_2, \tag{12}$$

that is,

$$\Delta\boldsymbol{d} = \boldsymbol{J}\Delta\boldsymbol{q}, \tag{13}$$

where

$$\boldsymbol{J} = [\ \boldsymbol{J_{\beta_1}}\ \boldsymbol{J_{\beta_2}}\ ], \tag{14a}$$

$$\Delta\boldsymbol{q} = [\ \Delta\beta_1\ \Delta\beta_2\ ]^T, \tag{14b}$$

with

$$\boldsymbol{J_{\beta_1}} = \begin{bmatrix} \frac{\partial x_{O_3}}{\partial\beta_1} \\ \frac{\partial y_{O_3}}{\partial\beta_1} \end{bmatrix} = \begin{bmatrix} \frac{l_{GE}\cos\gamma_1\sin(\beta_1+\delta)}{\sin^2\delta} \\ \frac{l_{GE}\sin\gamma_1\sin(\beta_1+\delta)}{\sin^2\delta} \end{bmatrix},$$

$$\boldsymbol{J_{\beta_2}} = \begin{bmatrix} \frac{\partial x_{O_3}}{\partial\beta_2} \\ \frac{\partial y_{O_3}}{\partial\beta_2} \end{bmatrix} = \begin{bmatrix} \frac{l_{GE}\sin\beta_1\cos(\gamma_1+\delta)}{\sin^2\delta} \\ \frac{l_{GE}\sin\beta_1\sin(\gamma_1+\delta)}{\sin^2\delta} \end{bmatrix}.$$

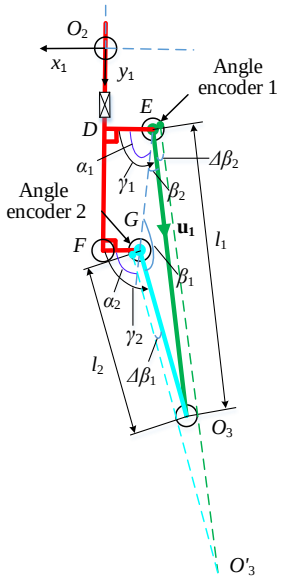

Fig. 6. Error model for the original measurement method.

B. A Measurement Method with Enhanced Accuracy

A new measurement method is proposed in connection with the 3-RPR mechanism, as shown in Fig. 7. An absolute angle encoder is installed at the joint located at F and a grating encoder sensor at FH. The angle encoder measures the angle value of θ_2 and the grating encoder sensor measures the length of FH. The location of $O_3(x_{O_3}, y_{O_3})$, l_1 and l_2 can be determined by (7) and (4).

Upon differentiation of (7), the positioning error of point O_3 can be obtained and reformulated as

$$\Delta\boldsymbol{d} = \boldsymbol{H_{l_{FH}}}\,\Delta l_{FH} + \boldsymbol{H_{l_{HO_3}}}\Delta l_{HO_3} + \boldsymbol{H_{\theta_2}}\Delta\theta_2 + \boldsymbol{H_s}\Delta s, \tag{15}$$

where Δs stands for the position error of point F. As Δl_{HO_3} and Δs are geometric errors, they can be eliminated by adjusting parameters. To simplify the analysis, only Δl_{FH} and $\Delta\theta_2$ are taken into consideration for further analysis. Equation (15) can be reformulated as

$$\Delta\boldsymbol{d} = \boldsymbol{H_{l_{FH}}}\,\Delta l_{FH} + \boldsymbol{H_{\theta_2}}\Delta\theta_2 \tag{16}$$

or

$$\Delta\boldsymbol{d} = \boldsymbol{H}\Delta\boldsymbol{p}, \tag{17}$$

where

$$\boldsymbol{H} = [\boldsymbol{H_{l_{FH}}}\ \ \boldsymbol{H_{\theta_2}}], \tag{18a}$$

$$\Delta\boldsymbol{p} = [\Delta l_{FH}\ \ \Delta\theta_2]^T, \tag{18b}$$

with

$$\boldsymbol{H_{l_{FH}}} = \begin{bmatrix} \frac{\partial x_{O_3}}{\partial l_{FH}} \\ \frac{\partial y_{O_3}}{\partial l_{FH}} \end{bmatrix} = \begin{bmatrix} -\sin\theta_2 \\ \cos\theta_2 \end{bmatrix},$$

$$\boldsymbol{H_{\theta_2}} = \begin{bmatrix} \frac{\partial x_{O_3}}{\partial\theta_2} \\ \frac{\partial y_{O_3}}{\partial\theta_2} \end{bmatrix} = \begin{bmatrix} l_{HO_3}\sin\theta_2 - l_{FH}\cos\theta_2 \\ -l_{HO_3}\cos\theta_2 - l_{FH}\sin\theta_2 \end{bmatrix}.$$

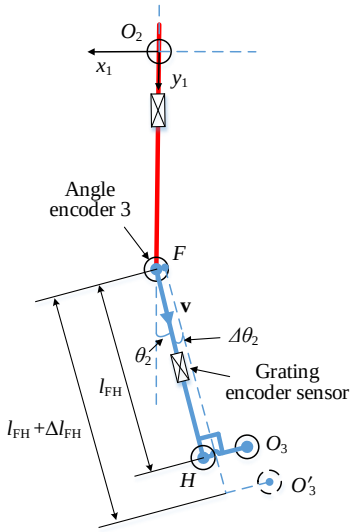

Fig. 7. Error model for the new measurement method.

This article has been accepted for publication in a future issue of this journal, but has not been fully edited. Content may change prior to final publication. Citation information: DOI 10.1109/TMECH.2018.2872011, IEEE/ASME Transactions on Mechatronics

C. Analysis of the Error Model

The measurement error of the knee joint driving point O_3 depends on the sensor accuracy and is associated with the Jacobian matrix.

The determinants of the Jacobian matrices $\boldsymbol{J}$ and $\boldsymbol{H}$ are given as

$$|\boldsymbol{J}| = \frac{{l_{GE}}^2 \sin(\beta_1 + \delta)\sin\beta_1}{\sin^3\delta}. \tag{19}$$

$$|\boldsymbol{H}| = l_{FH}. \tag{20}$$

It can be seen from (13) and (17) that the magnitude of the errors $\Delta\boldsymbol{d}$ is affected by the determinants of $\boldsymbol{J}$ and $\boldsymbol{H}$ that signify the ratio of the output and input errors. To avoid configuration singularity, $|\boldsymbol{J}| \neq 0$, which requires $\sin\beta_1 \neq 0$. From (19), we know that if $\delta \to 0$, $|\boldsymbol{J}| \to \infty$. Thus, (13) implies that if there is a small change in $\Delta\boldsymbol{q}$, there will be a large change in $\Delta\boldsymbol{d}$. On the contrary, the determinant of $\boldsymbol{H}$ is bounded, (17) implies that the error $\Delta\boldsymbol{d}$ can thus be controlled in a certain range acceptable for the system.

Turning to (10), we can see that the values of $\sin\beta_i$, $\cos\gamma_i$ and $\sin\gamma_i$ are bounded. In order to make the exoskeleton compact, l_{GE} should be small. Therefore the value of $1/\sin\delta$ should be large enough to satisfy the working stroke of point O_3. In order to realize this, δ should be small, but this leads to the result $\Delta\boldsymbol{d}$ being sensitive to $\Delta\boldsymbol{q}$. As the Jacobian matrix $\boldsymbol{H}$ is not singular, the value of $\Delta\boldsymbol{d}$ is not sensitive to $\Delta\boldsymbol{p}$.

To further simplify the error analysis, all the sensor inaccuracies are assumed to be identical, that is, $\Delta\beta_1 = \Delta\beta_2 = \Delta\theta_2 = \Delta\varphi$. Therefore, the measurement error by the original method is given as

$$\Delta\boldsymbol{d}_o = \boldsymbol{J}[\Delta\varphi\ \Delta\varphi]^T. \tag{21}$$

The measurement error by the new method is

$$\Delta\boldsymbol{d}_n = \boldsymbol{H}[\Delta\varphi\ \Delta l_{FH}]^T. \tag{22}$$

The position error of point O_3 can be defined as

$$\Delta d = \sqrt{({\Delta x_{O_3}}^2 + {\Delta y_{O_3}}^2)}. \tag{23}$$

The ratio k of the error magnifications between the new and original measurement is given as

$$k = \frac{\Delta d_n}{\Delta d_o}. \tag{24}$$

Combining (21)-(24), the ratio k can be obtained as

$$k = C_1 C_2 \sin^2\delta, \tag{25}$$

with

$$C_1 = \sqrt{[\left(l_{HO_3}\Delta\varphi - \Delta l_{FH}\right)^2 + (l_{FH}\Delta\varphi)^2]/(l_{GE}\Delta\varphi)^2} \quad \text{and}$$

$$C_2 = 1/\sqrt{\sin^2(\beta_1+\delta) + \sin^2\beta_1 + 2\sin(\beta_1+\delta)\sin\beta_1\cos\delta}.$$

We assume that $l_{HO_3}\Delta\varphi$ and Δl_{FH} are equal in magnitude, which leads to

$$C_1 = l_{FH}/\,l_{GE}. \tag{26}$$

As both C_1 and C_2 are bounded, if δ is small enough, the ratio k will be near zero. This implies that the new measurement method leads to smaller error than the original one.

With these error models, simulations based on MATLAB/ SimMechanics were conducted. Details of these are described in Section V, where the advantages of the new measurement method are presented.

IV. Closed-loop Control Law of the Exoskeleton

A closed-loop control of the exoskeleton has been implemented. A PID controller has been developed, as illustrated in Fig. 8.

The actual trajectory of the exoskeleton is measured by sensors. According to the error analysis in Section III, there are discrepancies between the measurement trajectory and the actual trajectory which is expressed as Δl_i in Fig. 8. These discrepancies will lead to inaccurate signals in the exoskeleton closed-loop control.

The PID controller is:

$$\begin{aligned} u(t) &= K_p\left[e(t) + \frac{1}{T_i}\int_0^t e(t)\,dt + T_d\frac{de(t)}{dt}\right] \\ &= K_p e(t) + K_i\int_0^t e(t)\,dt \ + K_d\frac{de(t)}{dt}, \end{aligned} \tag{27}$$

where K_p, K_i, K_d are the proportional, integral and differential gains.

In this exoskeleton, the motion error is defined as

$$e(t) = l_{i\_Ref} - l_{i\_Meas}\,,\ \ i = 0,1,2, \tag{28}$$

where l_{i_Ref} and l_{i_Meas}, i = 0, 1, 2, are the reference and measured trajectory of the three linear actuators, respectively.

l_{i_Meas} is given as

$$l_{i\_Meas} = l_{i\_act.} + \Delta l_i,\ \ i = 0,1,2, \tag{29}$$

where $l_{i\_act.}$, $i = 0,1,2$, is the actual lengths of actuation. $\Delta l_i, i = 0,1,2$, is the measurement error of the lengths of actuation. l_{i_Meas}, $i = 0,1,2$, is obtained by inverse kinematic calculation of the exoskeleton, as shown in (2) and (4).

Equations (28) and (29) yield

$$e(t) = l_{i\_Ref} - l_{i\_act.} - \Delta l_i\,, i = 0,1,2. \tag{30}$$

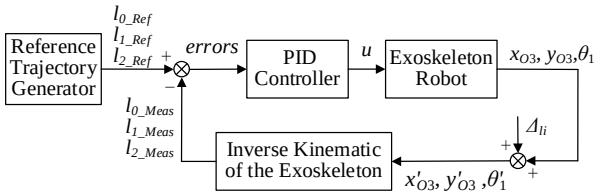

Fig. 8. Closed-loop control diagram of the exoskeleton robot.

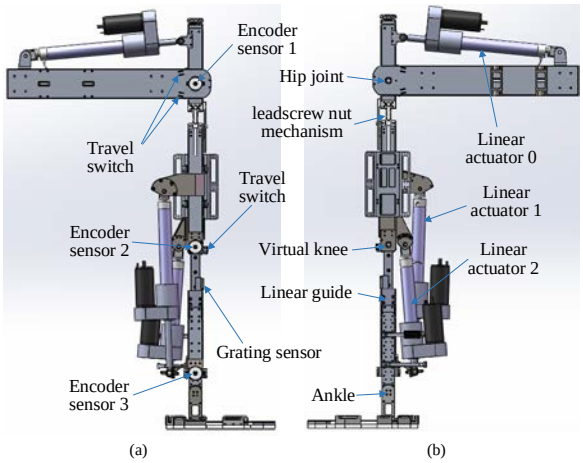

Fig. 9. Mechanical design of the exoskeleton: (a) front view, (b) rear view.

This article has been accepted for publication in a future issue of this journal, but has not been fully edited. Content may change prior to final publication. Citation information: DOI 10.1109/TMECH.2018.2872011, IEEE/ASME Transactions on Mechatronics

V. Simulations with MATLAB/SimMechanics

The mechanism model of the exoskeleton was built in SolidWorks, as shown in Fig. 9. The model is then imported into SimMechanics. In the simulation model, the input signals are the trajectories of the three actuators generated by MATLAB according to the general human gait [32]. The exoskeleton will move in a humanized way which considers the bionic knee joint under these trajectories. Details of this exoskeleton and gait will be described in Section VI. Because the actuators for the hip joint and knee joint are independent, as analyzed previously in Section III, the effect from the hip joint part is eliminated and the value of θ_1 is considered as zero.

A. Simulations with the Original Measurement Method

With the original measurement method, β_1 and β_2 are measured by angle sensors, and then the lengths of l_1 and l_2 and the position of O_3 can be calculated by using (8) and (10). As analyzed in Section III, measurement errors exist. Thus, we apply sinusoidal disturbing signals in the simulation to simulate this condition. The amplitudes of both signals are 0.01 rad (0.57°), and the frequencies of the two signals are 3Hz and 1Hz, respectively. The simulation results are shown in Fig. 10.

B. Simulations with the Alternative Measurement Method

With the alternative measurement method, the values of θ_2 and l_{FH} can be obtained with the help of an angle sensor and a grating sensor. The same disturbing signals as described in the previous section are added to this simulation. The amplitudes of angle errors are set to 0.01rad, and the amplitudes of length errors are 1mm. Simulation results are shown in Fig. 11.

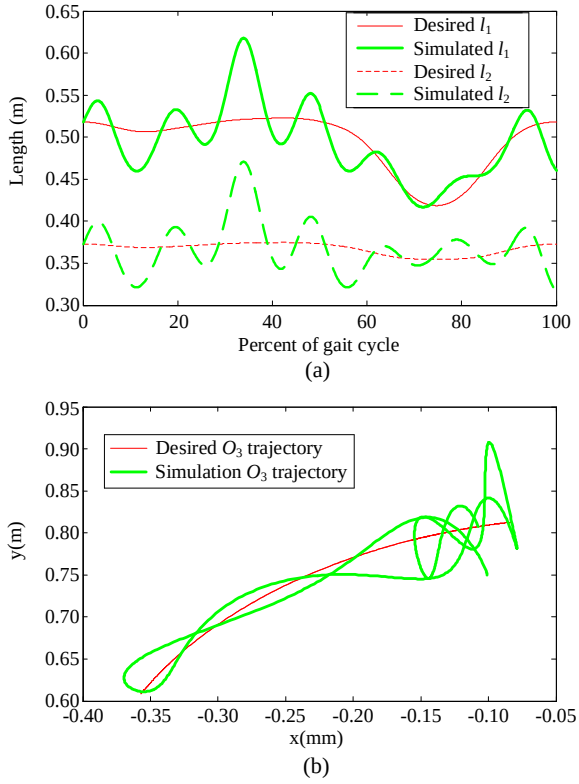

Fig. 10. Simulation results using the original measurement method with disturbance: (a) l_1 and l_2, (b) O_3 trajectory.

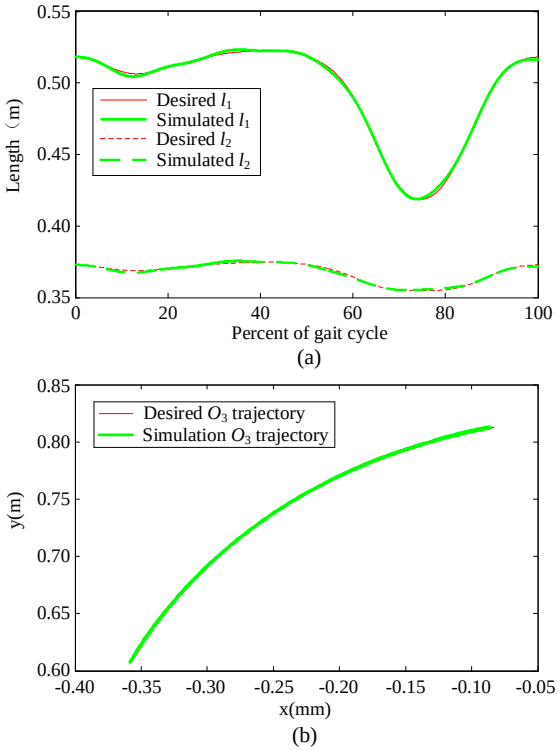

Fig. 11. Simulation results using the alternative measurement method with disturbance: (a) l_1 and l_2, (b) O_3 trajectory.

C. Analysis of the Simulation Results

The simulation results for the original method in Fig. 10 show that although the disturbances are very small (less than 0.57°) in the sensors, the measurement errors of lengths l_1 and l_2 and position O_3 are very large. In the simulated case, the maximum error is equal to 96.7 mm, which is not acceptable.

With our proposed method, the measurement errors of lengths l_1 and l_2 and position O_3 are significantly reduced, as shown in Fig. 11. For the simulated case, the maximum error is 4.2mm, which is considerably improved and acceptable, comparing with the original method.

This improvement agrees with the analysis of the error models in Section III. The measurement errors Δl_i with the alternative method are far less sensitive to the disturbances than with the original method. Therefore, it is reasonable to draw the conclusion that the proposed alternative measurement method is more suitable for a better control of the exoskeleton than the original method.

VI. Experiments

An experimental system of the BLLE-3 was developed, as shown in Fig. 12. It includes a host computer, a target computer, a body weight support, a treadmill and the exoskeleton. High level control of the exoskeleton is implemented via a user interface running on the host computer. The desired trajectory is generated and transferred to the target computer by the host computer. The target computer consists of a digital signal processor (DSP) and a field-programmable gate array (FPGA). The DSP is used to control the motors via a Controller Area Network (CAN) field-bus. It also communicates with the host computer by a serial port communication. The FPGA is used to process the data

This article has been accepted for publication in a future issue of this journal, but has not been fully edited. Content may change prior to final publication. Citation information: DOI 10.1109/TMECH.2018.2872011, IEEE/ASME Transactions on Mechatronics

from the sensors and to communicate with the DSP by a parallel port communication. The exoskeleton includes two limbs. One is developed as shown in Fig. 13, which can be considered as the bionic knee joint exoskeleton, and the other is designed to be similar to the Lokomat [14], the hip and knee joints of which are actuated and considered as a rotation DOF. The two limbs are designed differently for different testing in the future. The bionic knee joint exoskeleton has three 17-bit absolute encoders (AD36/1217AF. ORBVB, Hengstler, Germany), one grating sensor (O. P. S. Series 20, MicroE Systems, USA), three linear actuators with 500 CPT embedded encode sensor (RE50, Part Number: 370356, Maxon DC motor, Switzerland) and three motor drives (Accelnet Micro- Panel, ACJ-055-18, Copley, USA). Encoder 1 is used for recording the angle of the hip joint and Encoders 2 and 3 together record the angle of the knee joint. The length of the shank is measured by the grating sensor. This exoskeleton leg fits patients from 1.60m to 1.90m tall, which covers more than 90% of corresponding adult males [33], with a maximum body weight of 100kg. The exoskeleton is designed according to the statistics in which the normal ranges of walking are about 20˚ in flexion and 30˚ in extension for the hip joint, and about 60˚ in flexion and 0˚ in extension for the knee joints [32]. The specifications are applicable for walking on level ground and the influence of terrains such as slope or stairs [34] is not considered in this study.

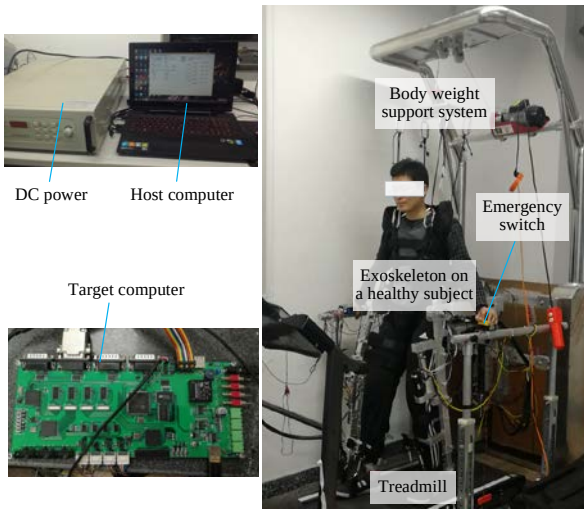

Fig. 12. Overview of the BLLE-3 system.

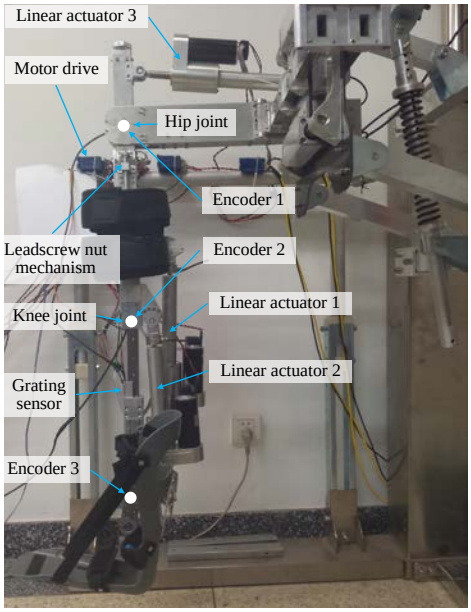

Fig. 13. Prototype of the bionic knee joint exoskeleton.

A. Experimental Setup

Experiments were conducted to demonstrate the functionality of the new system. Two healthy subjects (A and B, age 23 and 25, weight 65kg and 68kg, height 179cm and 180cm) were recruited for path-tracking experiments. Written consents were obtained from them. Each subject was instructed to conduct three different trajectories. For safety reasons, the maximum speed and acceleration of the actuators are limited by the software and the exoskeleton will stop moving if the interaction force between the exoskeleton and the wearer is greater than an allowable value. Besides, the subjects were allowed to shut off the power with an emergency stop if they needed to do so at any time, as shown in Fig. 12.

Trajectories for the hip and knee joints are defined according to the statistical data of general human gait [32]. For the first path L_1, the knee joint is considered as a pin joint, thus the length of *FH* is fixed. For the other two paths L_2 and L_3, the bionic knee joint is taken into consideration, and the *FH* length changes with the angle θ_2.

Path L_2 follows a trajectory defined with

$$l_{FH} = l_0 + \frac{45\theta_2}{1000\pi}, \tag{31}$$

Moreover, path L_3 follows another trajectory defined with

$$l_{\mathrm{FH}} = l_0 + \frac{18\sin\theta_2}{1000}, \tag{32}$$

where l_{FH} unit is m, and θ_2 unit is in radian, and l_0 is the initial length of *FH* when $\theta_2 = 0$. l_0 is set as 0.375m for subject A and 0.376m for subject B.

The reference trajectories for the three linear actuators can be obtained by kinematical calculation as analyzed in Section II. During the experiment, θ_1, θ_2 and l_{FH} values were obtained by encoders 1 and 2 and the grating sensor, respectively. Then the actual trajectories of the three linear actuators were calculated by kinematical solutions. The exoskeleton was controlled by the closed-loop control law with a PID controller, as shown in Fig. 8.

B. Experimental Results

A good agreement between the reference and real trajectory shows the effectiveness of the new measurement and control method. Typical trajectory's tracking results are shown in Fig. 14. The maximum errors of θ_1 and θ_2 are less than 1.6°, and the maximum error of l_{FH} is less than 1.2mm.

The main feature of BLLE-3 is the bionic knee joint design which can suit the knee joint translation and the rotational movement. This feature is achieved by the adjustment of l_{FH} according to the knee joint rotation angle θ_2. The length adjustment error in path tracking is defined as

$$dl_{FH}(t) = l_{FH\_act.} - l_{FH}\big(\theta_2(t)\big), \tag{33}$$

where $l_{FH}\big(\theta_2(t)\big)$ is the reference value of l_{FH} according to the actual knee joint angle θ_2, and $l_{FH\_act.}$ is the actual length of *FH* during the leg motion.

This article has been accepted for publication in a future issue of this journal, but has not been fully edited. Content may change prior to final publication. Citation information: DOI 10.1109/TMECH.2018.2872011, IEEE/ASME Transactions on Mechatronics

The error of varying length l_{FH} in the motion assistance task is shown in Fig. 15. The maximum error is 0.723 mm.

The varying length l_{FH} tracking errors in all tasks are listed in Table I. As it shows, most tracking errors are within 0.3mm and the maximum error is 0.976 mm.

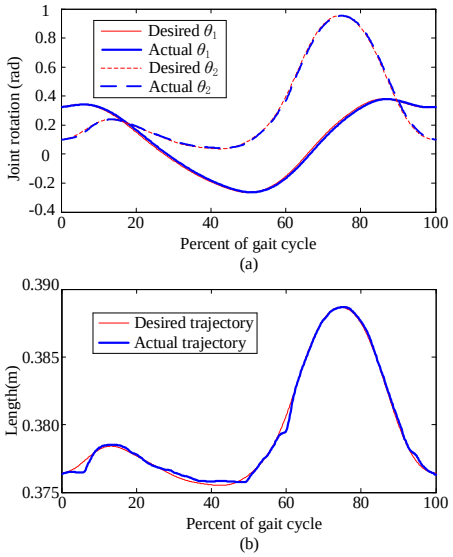

Fig. 14. Experimental trajectories tracking results: (a) θ_1 and θ_2, (b) l_{FH} (Subject A, Path L_2).

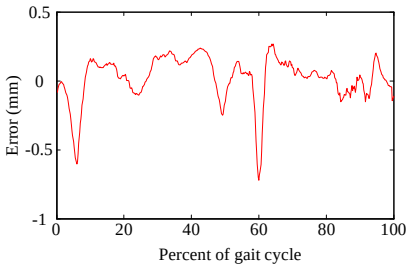

Fig. 15. A typical l_{FH} tracking error (Subject A, Path L_2).

TABLE I
TRAJECTORY TRACKING RESULTS

Subject	Path	Mean	Std. Deviation	Max. / Min.
A	L_1	0.018mm	0.220mm	0.432mm/-0.816mm
	L_2	0.021mm	0.166mm	0.266mm/-0.723mm
	L_3	0.025mm	0.128mm	0.217mm/-0.533mm
B	L_1	0.011mm	0.461mm	0.976mm/-0.696mm
	L_2	-0.001mm	0.300mm	0.592mm/-0.743mm
	L_3	-0.009mm	0.273mm	0.541mm/-0.638mm

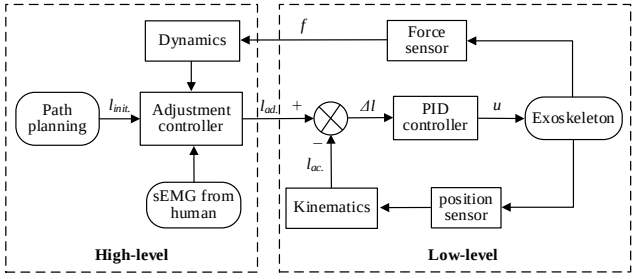

Fig. 16. Two level structure controller.

VII. DISCUSSION

It has been noted that experiments on Lokomat show that the mean value of misalignment between the human and exoskeleton knee joints in the sagittal plane is about 12mm, and the maximum misalignment can exceed 20mm over the mean gait cycle [35], [36]. With our design, a significant reduction in the misalignment can be expected. It is noted that our current results are not able to show directly the actual misalignment due to a lack of experimental conditions in which we could detect the skeletal positions of the human lower limb. Further testing in collaboration with doctors in clinical labs should be considered for this purpose.

The 3-RPR parallel mechanism uses two linear actuators to adapt to the knee joint misalignment. Compared with most lower limb exoskeletons in which the knee joint has been designed to be a pin joint, the new exoskeleton can potentially overcome the knee joint misalignment problem. However, this new design makes the whole system more complex. Fortunately, as can be seen in Fig. 12, for our treadmill-based exoskeleton, the weight of the exoskeleton can be passed to the ground by the base. Besides, the control of a 2-DOF parallel mechanism is also a mature technology. Thus, the inclusion of an additional actuator for the knee joint does not create much difficulty for both the control and the cost of the exoskeleton.

In this work, the 3-PRP parallel mechanism is analyzed with geometric approach. It can also be analyzed algebraically by resorting to other approaches with multi-loop kinematic chains or multi-body kinematics [37]. All approaches can readily yield the same kinematic solutions.

From the experiment, it can be seen that the coupling motion trajectory of the human knee joint is hard to generate to ensure there is no relative displacement between the exoskeleton and the wearer during the gait cycle. To overcome this problem, a two-level structure controller is proposed for future implementation, as shown in Fig. 16. In the high-level, interaction force (especially parasitic force) will be used as one of the main control signals, and the trajectories will be adjusted online. The low-level will direct the exoskeleton to follow the reference trajectories transferred from the high-level. It will be an interesting task in future works to determine the trajectories according to the interaction force.

As seen in Fig.16, it is a two-level structure controller. The low-level is responsible for executing the trajectories transferred from the high-level. Thus, a position controller in the low-level is workable for the control. While the high-level is to generate the reference trajectories, a force controller will be considered in the high-level for the generation of a suitable trajectory for the wearer. In this paper, our focus is on the low-level, and a PID based position controller has been developed for precise trajectory control. Further work about the high-level controller and the force feedback information will be taken into consideration.

VIII. CONCLUSION

This paper presents a biologically inspired lower limb exoskeleton which can fully accommodate the movement of the human knee joint for human gait rehabilitation. The exoskeleton was built with a 3-RPR parallel mechanism which was used as a precise measurement mechanism to obtain the trajectory of the lower limb to perform a closed-loop control. Error models of the exoskeleton were built and analyzed. A closed-loop control law

was developed for a precise trajectory control. Simulations with Matlab/SimMechanics have shown that the new measurement method enhances performance of trajectory tracking. Experimental results have demonstrated the effectiveness of the new measurement and control method.

A major contribution of the work lies in the new mechatronic design of the exoskeleton leg, which incorporates parallel kinematics and precision measurement with error analysis. This enables a precise closed-loop control for trajectory tracking. The new design improves physical human-robot interaction with a better alignment between the human and exoskeleton joints.

Another contribution of the work is the experimental validation of the accurate trajectory control for rehabilitations, which justifies the potential in improving trajectory tracking performance with the new system. Future work will focus on dynamics and human-exoskeleton interaction analysis. The interaction force between the human lower limb and the exoskeleton will be obtained and analyzed. Motion trajectories will be determined online to adapt them to the joint misalignments. sEMG signals will also be measured in order to assess patients' conditions.

ACKNOWLEDGMENT

The authors would like to thank Prof. Mark Buck for proofreading and Xin Chen, Xuan Yi for their help during the fabrication and experiments of the BLLE-3.

REFERENCES

[1] R. Camicioli, M. M. Moore, G. Sexton, D. B. Howieson, and J. A. Kaye, "Age-related brain changes associated with motor function in healthy older people," *J. Am. Geriatr. Soc.*, vol. 47, no. 3, pp. 330-334, 1999.

[2] N. A. Bayona, J. Bitensky, K. Salter, and R. Teasell, "The role of task-Specific training in rehabilitation therapies," *Top. Stroke Rehabil*. vol. 12, no. 3, pp.58-65, 2005.

[3] W. Meng, Q. Liu, Z. Zhou, Q. Ai, B. Sheng, and S. Xie, "Recent development of mechanisms and strategies for robot-assisted lower limb rehabilitation," *Mechatronics*, vol. 31, pp. 132-145, 2015.

[4] T. G. Sugar, D. Armstrong, B. Najafi, S. Redkar and J. A. Ward, "Low-limb wearable robotics" in *Wearable Exoskeleton Systems: Design, Control and Applications*, S. Bai, G. S. Virk and T. Sugar, Eds. Institution of Engineering & Technology, 2018, pp. 5-16.

[5] K. H. Low, "Robot-Assisted Gait Rehabilitation: From Exoskeletons to Gait Systems," *in Proc. Defense Science Research Conf. and Expo*, Singapore, Aug. 3-5, 2011, pp.1-10.

[6] Y. Chen, J. Hu, F. Zhang, Z. Hou, "Simulation Study of an FES-Involved Control Strategy for Lower limb Rehabilitation Robot," in *Intelligent Robotics and Applications*, CY. Su, S. Rakheja, H. Liu, Eds. ICIRA, Spring, Berlin, Heidelberg, 2012, pp. 85-95.

[7] PY. Cheng, and PY. Lai, "Comparison of exoskeleton robots and end-effector robots on training methods and gait biomechanics," in *Intelligent Robotics and Applications*, J. Lee, et al. Eds. ICIRA, Spring, Berlin, Heidelberg, 2013, pp. 258-266.

[8] S. Hesse, and D. Uhlenbrock, "A mechanized gait trainer for restoration of gait," *J. Rehabil. Res. Dev.*, vol. 37, no. 6, pp. 701-708, 2000.

[9] H. Yano, K. Kasai, H. Saito, and H. Iwata, "Sharing sense of walking with locomotion interfaces," *Int. J. Hum.-Comput. Interact.*, vol. 17, no. 4, pp. 447-462, 2009.

[10] H. Schmidt, S. Hesse, R. Bernhardt, and J. Kruger, "HapticWalker—A Novel Haptic Foot Device," *ACM Trans. Appl. Percept.*, vol. 2, no. 2, pp. 166 – 180, 2005

[11] S. Hesse, A. Waldner, and C. Tomelleri, "Innovative gait robot for the repetitive practice of floor walking and stair climbing up and down in stroke patients," *J. Neuroeng. Rehabil.*, vol. 7, no. 30, 2010

[12] B. W. Ko, and W. K. Song, "Kinematic Comparison of Gait Rehabilitation with Exoskeleton and End-Effector Devices," in *Wearable Robotics: Challenges and Trends. Biosystems & Biorobotics*, vol. 16. J. G. Vargas et al. Eds. Springer, Cham, 2017, pp. 213-217.

[13] J. Mehrholz, and M. Pohl, "Electromechanical-assisted gait training after stroke: A systematic review comparing end-effector and exoskeleton devices," *J. Rehabil. Med.* vol. 44, no. 3, pp. 193-199, 2012.

[14] S. Jezernik, G. Colombo, M. Morari, "Automatic Gait-Pattern Adaptation Algorithms for Rehabilitation With a 4-DOF Robotic Orthosis," *IEEE Trans. Robotics and Automation*, vol. 20, no. 3, pp. 574-582, 2004.

[15] B. Koopman, E. H. F. Asseldonk and H. Kooij, "Estimation of Human Hip and Knee Multi-Joint Dynamics Using the LOPES Gait Trainer," *IEEE Trans. Robot.*, vol. 32, no. 4, pp. 920 – 932, 2016.

[16] Y. Stauffer, Y. Allemand, M. Bouri, J. Fournier, R. Clavel, P. Metrailler, R. Brodard, and F. Reynard, "The WalkTrainer—A New Generation of Walking Reeducation Device Combining Orthoses and Muscle Stimulation," *IEEE Trans. Neural Syst. Rehabil. Eng.*, vol. 17, no. 1, pp. 38-45, 2009.

[17] D. Zanotto, P. Stegall, and S. K. Agrawal, "ALEX III: A Novel Robotic Platform with 12 DOFs for Human Gait Training," *in Proc. IEEE Int. Conf. Robot. Autom.*, Karlsruhe, Germany, May 6-10, 2013, pp. 3914-3919.

[18] M. Talaty, A. Esquenazi, and J. E. Briceño, "Differentiating Ability in Users of the Rewalk™ Powered Exoskeleton: An analysis of walking kinematics," *in Proc. IEEE Int. Conf. on Rehabil. Robot.*, Seattle, WA, Jun. 24-26, 2013, pp.1-5.

[19] T. Ueba, O. Hamada, T. Ogata, T. Inoue, E. Shiota, and Y. Sankai, "Feasibility and safety of acute phase rehabilitation after stroke using the hybrid assistive limb robot suit," *Neurol. Med.-chir.*, vol. 53, no. 5, pp. 287-290, 2013.

[20] A. Schiele and F. van der Helm, "Kinematic design to improve ergonomics in human machine interaction," *IEEE Trans. Neural Syst. Rehabil. Eng.*, vol. 14, no. 4, pp. 456–469, 2006.

[21] H. Iwaki, V. Pinskerova, and M. A. R. Freeman, "Tibiofemoral movement 1: the shapes and relative movements of the femur and tibia in the unloaded cadaver knee," *J. Bone Joint Surg.*, vol. 82-B, no. 8, pp. 1189 –1195, 2000.

[22] K. M. Lee, J. Guo, "Kinematic and dynamic analysis of an anatomically based knee joint," *J. Biomech.*, vol. 43, no. 7, pp. 1231-1236, 2010.

[23] B. Celebi, M. Yalcin, and V. Patoglu, "Assist On-Knee: A self-aligning knee exoskeleton," *in Proc. IEEE/RSJ Int. Conf. Intell. Robots Syst.*, Tokyo, Japan, Nov. 3-7, 2013, pp. 996–1002.

[24] Y. Lee, Y. J. Kim, J. Lee, M. Lee, B. Choi, J. Kim, Y. J. Park and J. Choi, "Biomechanical Design of a Novel Flexible Exoskeleton for Lower Extremities," *IEEE/ASME Trans. Mechatronics*, vol.22, no.5, pp. 2058-2069, 2017.

[25] F. Patané, S. Rossi, F. D. Sette, J. Taborri, and P. Cappa, "WAKE-Up Exoskeleton to Assist Children With Cerebral Palsy: Design and Preliminary Evaluation in Level Walking," *IEEE Trans. Neural Syst. Rehabil. Eng.*, vol. 25, no. 7, pp. 906-916, 2017.

[26] D. Zanotto, Y. Akiyama, P. Stegall, S. K. Agrawal, "Knee Joint Misalignment in Exoskeletons for the Lower Extremities: Effects on User's Gait," *IEEE Trans. Robot.*, vol. 31, no. 4, pp. 978 – 987, 2015.

[27] M. A. Ergin, and V. Patoglu, "A Self-Adjusting Knee Exoskeleton for Robot-Assisted Treatment of Knee Injuries," *in Proc. IEEE/RSJ Int. Conf. Intell. Robots Syst.*, San Francisco, CA, Sept. 25-30, 2011, pp. 4917-4922.

[28] D. Wang, K. M. Lee, J. Guo, C. Yang, "Adaptive Knee Joint Exoskeleton Based on Biological Geometries," *IEEE/ASME Trans. Mechatronics*, vol. 19, no. 4, pp. 1268-1278, 2014.

[29] M. Lyu, W. Chen, X. Ding, J. Wang, S. Bai, and H. Ren, "Design of a biologically inspired lower limb exoskeleton for human gait rehabilitation," *Rev. Sci. Instrum.*, vol. 87, 10431, pp. 1- 13, 2016.

[30] D. A. Dennis, and R. D. Komistek, "Kinematics of Mobile Bearing Total Knee Arthroplasty," in *Total Knee Arthroplasty: A Guide to Get Better Performance*, J. Bellemans, M. D. Ries, J. M. K. Victor, Eds. Heidelberg, Germany: Springer Medizin, 2005. pp. 126-140.

[31] D. Corradi, S. Caro, D. Chablat, and P. Cardou, "Assembly Conditions of Parallel Manipulators Considering Geometric Errors, Joint Clearance, Link Flexibility and Joint Elasticity," *in Proc. IEEE Int. Conf. Robot. Autom.*, Hong Kong, China, May 31 – Jun. 7, 2014, pp. 4067-4072.

[32] J. Perry MD, *Gait Analysis: Normal and Pathological Function*, Slack Incorporated, Thorofare, 1992, pp. 309-311.

[33] R. L. Huston, *Principles of Biomechanics*, CRC Press, Boca Raton, 2009, pp. 24-26.

[34] J. Jang, K. Kim, J. Lee, B. Lim, J. K. Cho, and Y. Shim, "Preliminary study of online gait recognizer for lower limb exoskeletons," in *Proc. IEEE/RSJ Int. Conf. Intell. Robots Syst.*, Vancouver, Canada, Sept. 24-28, 2017, pp. 5818–5824.

[35] J. Hidler, W. Wisman, and N. Neckel, "Kinematics trajectories while walking within the Lokomat robotic gait-orthosis," *Clin. Biomechs*, vol. 23, no. 10, pp. 1251-1259, 2008.

[36] N. Neckel, W. Wisman, and J. Hidler, "Limb alignment and kinematics inside a lokomat robotic orthosis," *in Proc. IEEE EMBS Annual Int. Conf.*, New York, USA, Aug. 30-Sept. 3, 2006, pp. 2698-2701.

[37] N. Jarrasse and G. Morel, "Connecting a Human Limb to an Exoskeleton", *IEEE Trans. Robot.*, vol. 28, no. 3, pp. 697 – 709, 2012.

Libo Zhou received the B.S. degree in mechanical engineering and automation from the University of Science and Technology Beijing, Beijing, China, in 2015. He is currently working toward the Ph.D. degree in control science and engineering under the guidance of Prof. Weihai Chen at Beihang University, Beijing, China.

He was a visiting student at National University of Singapore under the guidance of Prof. Haoyong Yu from March 2017 to July 2017. His research interests include rehabilitation robotics and exoskeletons.

Weihai Chen (M'00) received the B.S. degree in detection technology from Zhejiang University, Hangzhou, China, in 1982, and the M.S. and Ph.D. degree in mechanical engineering from Beihang University, Beijing, China, in 1988 and 1996, respectively.

He became an Associate Professor in 1998 and a Professor in 2007 with Beihang University, where he is currently the Director of the Intelligent Robotics and Measurement and Control Technology Laboratory. His research interests include bio-inspired robotics, micro-manipulation, and computer vision.

Prof. Chen is a member of the Technical Committee on Manufacturing Automation of the IEEE Robotics and Automation Society, and a senior member of the Chinese Mechanical Engineering Society.

Jianhua Wang received the B.S. in electronic science and technology and M.S. degree in industrial automation from Beihang University, Beijing, China, in 1984 and 1987, respectively.

He is currently an Associate Professor with the School of Automation Science and Electrical Engineering, Beihang University. His research interests include bio-inspired robotics, robot control and autonomous navigation.

Shaoping Bai (M'01) received B.S. degree from Harbin Institute of Technology, Harbin, China, in 1988, the M.S. degree from Tsinghua University, Beijing, China, in 1993, and the Ph.D. degree in mechanical and production engineering from the Nanyang Technological University, Singapore, in 2001.

He is currently an Associate Professor at the Department of Materials and Production, Aalborg University (AAU), Denmark. His research interests include dynamics and design, medical and assistive robots, parallel manipulators, and walking robots. He is a member of ASME and IEEE Robotics and Automation and an Associate Editor of ASME J. Mechanisms and Robotics.

Haoyong Yu (M'10) received the Ph.D. degree in mechanical engineering from Massachusetts Institute of Technology, Cambridge, MA, USA, in 2002.

He is currently an Associate Professor with the Department of Biomedical Engineering and a Principal Investigator of the Singapore Institute of Neurotechnology (SINAPSE), National University of Singapore. His research interests include medical robotics, rehabilitation engineering and assistive technologies, and system dynamics and control. Dr. Yu received the Outstanding Poster Award at the IEEE Life Sciences Grand Challenges Conference 2013. He has served on a number of IEEE conference organizing committees.

Yinping Zhang received the B.S. degree in automation from Beijing Jiaotong University, Beijing, China, in 2016. She is currently working toward the M.S. degree in control science and engineering at Beihang University, Beijing, China.

Her research interests include rehabilitation robots, multi-information fusion, path planning and motion control.